Measuring Affinities of Fission Yeast Spindle Pole Body Proteins in Live Cells across the Cell Cycle

Chad D. McCormick,[†] Matthew S. Akamatsu,[†] Shih-Chieh Ti,[†] and Thomas D. Pollard[†‡§*]
[†]Departments of Molecular Biophysics and Biochemistry, [‡]Departments of Molecular Cellular and Developmental Biology, and [§]Department of Cell Biology, Yale University, New Haven, Connecticut

ABSTRACT Characterizing protein-protein interactions is essential for understanding molecular mechanisms, although reproducing cellular conditions in vitro is challenging and some proteins are difficult to purify. We developed a method to measure binding to cellular structures using fission yeast cells as reaction vessels. We varied the concentrations of Sid2p and Mob1p (proteins of the septation initiation network) and measured their binding to spindle pole bodies (SPBs), the centrosome equivalent of yeast. From our measurements we infer that Sid2p and Mob1p both exist as monomeric, heterodimeric, and homodimeric species throughout the cell cycle. During interphase these species have widely different affinities for their common receptor Cdc11p on the SPB. The data support a model with a subset of Cdc11p binding the heterodimeric species with a $K_d < 0.1$ μM when Sid2p binds Mob1p-Cdc11p and K_d in the micromolar range when Mob1p binds Sid2p-Cdc11p. During mitosis an additional species presumed to be the phosphorylated Sid2p−Mob1p heterodimer binds SPBs with a lower affinity. Homodimers of Sid2p or Mob1p bind to the rest of Cdc11p at SPBs with lower affinity: K_ds > 10 μM during interphase and somewhat stronger during mitosis. These measurements allowed us to account for the fluctuations in Sid2p binding to SPBs throughout the cell cycle.

INTRODUCTION

For over a century chemists and biochemists have quantified the interactions of molecules in vitro, perfecting protocols to determine the stability of certain reactions (1). Quantitative characterization of the interactions of biological macromolecules is essential for a complete understanding of any biological system. However, it is challenging to replicate in vitro all of the conditions that ligands encounter in a cellular environment, from molecular crowding to post-translational modifications. Here, we develop an approach to characterize interactions between proteins in a subcellular structure, the yeast spindle pole body (SPB), in the native environment throughout the cell cycle. This method complements existing biochemical and biophysical methods to better understand biochemical mechanisms in living cells.

The septation initiation network (SIN) of the fission yeast *Schizosaccharomyces pombe* is a cascade of signaling proteins that regulates cytokinesis (2–5). Many of the reactions among components of this pathway occur on the SPB, a complex of proteins that spans the inner and outer nuclear membranes and serves as both the microtubule organizing center for the mitotic spindle and a hub for cell cycle signaling. Cdc11p is the SPB receptor for the Sid2p kinase with its accessory protein Mob1p (6,7). Of the two SPBs in mitosis, the daughter SPB contains more activators of SIN (8–10). Activation of the SIN pathway during mitosis leads to phosphorylation of the Sid2p kinase (11). Active phosphorylated Sid2p phosphorylates substrates including Cdc11p (12), Clp1p (13), Fin1p (14), and potentially many others (15). Active Sid2p also migrates in a complex with Mob1p from the SPB to the cytokinetic contractile ring, where it initiates ring constriction and synthesis of cell wall material to form the septum (16). Ablation of the daughter SPB can lead to activation of the mother SPB (9).

Previous studies inferred the biochemical states of Sid2p at the SPB throughout the cell cycle. Heterodimers of Sid2p with Mob1p are the species activated by the SIN pathway and Mob1p is important for the association of Sid2p with SPBs, because no Sid2p appears to localize to SPBs in cells lacking Mob1p (17). Formation of homodimers was proposed to sequester Sid2p from Mob1p and the possibility of activation (16). Truncation mutations of Sid2p showed that its 207 N-terminal residues are sufficient for self-association and binding Mob1p and SPBs (16). Given these interactions of the N-terminus of Sid2p, it is expected a cytoplasmic pool of Sid2p includes a mixture of monomers, heterodimers, and homodimers available for binding to the SPB. Sid2p binds directly to SPBs by interacting with its receptor, the N-terminal 660 residues of Cdc11p (3,6).

Mob1p may also bind directly to Cdc11p given that Mob1p localizes to SPBs in temperature sensitive *sid2+* mutants (17,18). Mob1p forms soluble homodimers at high (700 μM) concentrations (19) but not at micromolar physiological concentrations in cells. A crystal structure of Mob1p dimers suggested that Sid2p binds on the opposite side of the protein from the homodimer interface (19).

Current methods to measure protein-protein interactions in cells use fluorescence correlation spectroscopy, fluorescence cross correlation spectroscopy, or Forster resonance energy transfer (FRET) (20–24). An advantage of these methods is their ability to track both binding species

Submitted April 8, 2013, and accepted for publication August 14, 2013.

*Correspondence: thomas.pollard@yale.edu

Editor: Rong Li.

0006-3495/13/09/1324/12 $2.00

http://dx.doi.org/10.1016/j.bpj.2013.08.017

simultaneously. In fluorescence correlation spectroscopy and fluorescence cross correlation spectroscopy a small cytosolic volume is used to determine the interaction of diffusing fluorescent ligands, but the methods do not typically provide useful data about immobile targets like the SPB. FRET detects specific pairs of fluorescent molecules, but may require intensive computation, spectral unmixing, and/or higher concentrations of fluorescent proteins to isolate the signal.

Here, we describe a complementary approach using quantitative fluorescence microscopy (8,25–27) to measure binding of fluorescent protein ligands to an organelle, the yeast SPB. We varied the concentrations of Sid2p or Mob1p ligand and measured binding to a constant number of Cdc11p receptors at the SPB to derive biophysical parameters of this three-component system throughout the cell cycle. These measurements validated and expand upon a previous model of the interactions among Sid2p, Mob1p, and Cdc11p (16). During interphase the Sid2p-Mob1p heterodimer binds a limited number of Cdc11p receptors at the SPB with high affinity. During mitosis the affinity of Sid2p-Mob1p for the SPB falls, presumably due to phosphorylation and translocation of the heterodimer to the contractile ring (16). During both interphase and mitosis most of the Cdc11p receptors on the SPB bind Sid2p and Mob1p with much lower affinities.

METHODS

Strain construction

The master segmentation strain CM184 (*sad1-2(TEV-mCFP)-natMX6 seh1-mCFP-hphMX6 ade6-M210 leu1-32 ura4-D18*) was constructed as follows. We cloned TEV-mCFP into a pFA6a-TEV-mCFP-kanMX6 vector to produce a plasmid with two copies of mCFP. We used standard methods to tag Sad1p with 2(TEV-mCFP)-kanMX6 in its chromosomal locus (28). We used antibiotic resistance switching polymerase chain reaction methods to replace the *kanMX6* resistance gene with *natMX6* (29). We used standard genetic methods to generate the *seh1-mCFP-hphMX6* strain. With these initial strains we made both mating types of the master segmentation strain. These strains grew like wild-type (WT) strains and were crossed with all subsequent *mYFP-kanMX6* strains. The different antibiotic resistances of the markers simplified progeny identification. *S. pombe* cells expressing mYFP-Sid2p or mYFP-Mob1p under the control of a *3nmt1*, *41nmt1*, or *81nmt1* promoter were crossed with the master segmentation strain to allow for semiautomatic segmentation of SPBs regardless of the contrast in the mYFP counting channel. For consistent quantitative results we crossed the calibration curve strains with the segmentation strain (Table S1 in the Supporting Material). We constructed additional strains for calibration experiments by standard methods (28).

Extended calibration curve experiments

We purified the ARPC1 subunit of the *S. pombe* Arp2/3 complex with a mYFP tag (Arc1p-mYFP) as a high molecular weight fluorescent standard from strain CB108 using ammonium sulfate precipitation, GST-WA affinity chromatography and anion exchange chromatography (30). We calculated the concentration of purified Arc1p-mYFP with the extinction coefficient of mYFP at 514 nm. We ran 0.01–0.05 pmol of Arc1p-mYFP on an immunoblot along with duplicate samples of extracts of cells expressing mYFP-tagged copies of various calibration proteins to measure the number of mYFP-tagged molecules in each strain (8). We used high-copy number housekeeping proteins tagged on their C-termini to extend the existing calibration curve (Fig. S1).

Protein induction and semiautomated microscopy

Cells were maintained in log phase growth for 36 h in liquid YE5S or YE5S medium with zero or 15 μM thiamine for a high expression of constructs. Cells were transferred to minimal media with zero or 15 μM thiamine for 16–29 h to extend the range of expression. To assure that the cells remained in log phase before imaging, OD_{595} was maintained below 0.5. Samples were imaged as in Wu et al. (25) with the following modifications. Samples were imaged at regular time intervals post-induction on a gelatin pad containing EMM5S medium with 250 nM Alexa 647 $\pm$15 μM thiamine. The counterstain dye was included in the calibration curve measurements to account for minimal bleed-through in the mYFP channel. Cells were imaged on an Andor Revolution XD Spinning Disk confocal microscope (Andor Technology, Belfast, UK) with a Yokogawa CSU-X head and Andor iXon+ 897 camera on an Olympus (Center Valley, PA) IX-71 microscope with an UPLSAPO 100XO 1.40 NA objective. We used Semrock (Rochester, NY) CFP/YFP emission filter Em01-R442/514/647-15 and the Cy5 emission filter Em01-R442/647-25. Cells were imaged with a five field, automated protocol: i), acquire a DIC image of a user-selected field with no gain, 3 s ramp up to 300 gain; ii), acquire images of Alexa 647 in 21 planes along 5.2 μm of the *Z* axis; iii), repeat Alexa 647 acquisition 1–4 additional times; iv), acquire a single quantitative stack of images in the mYFP channel; v); acquire a single stack of images in the mCFP segmentation channel ending in a 3 s delay; and vi), acquire a final DIC image. This entire acquisition process was repeated at four other user-selected stage positions. This protocol was repeated 2–3 times per slide to ensure maximum data collection. To maximize the dynamic range of the camera we tested the linear range of the camera and varied the exposure time (linear relationship) and laser intensity (nonlinear, which required an extra calibration curve) to ensure no pixel intensity values reached above ~80% of the maximum pixel intensity value. Size, position, and intensity were extracted from the micrographs to yield plots with apparent volume, numbers of molecules, and concentrations.

Semiautomatic image analysis

We created a macro in ImageJ (http://rsbweb.nih.gov/ij/) to detect cell edges automatically. We started with a time average of the sum intensity projection of the 647 nm excitation counterstain images. We applied a 5 pixel radius Gaussian blur to the image and used Laplacian-based edge detection to approximate the cell peripheries in these images (31). We then converted the detected cell peripheries to individual convex hulls given that none of our overexpression phenotypes produced bent or T-shaped cells. From our a priori knowledge of the size of *S. pombe* cells, we used ImageJ particle analysis with reasonable approximations for cell area and circularity to help remove outliers. We allowed for user input to edit and add cell selections manually.

To detect SPBs we first counted the number of nuclei present in each cell using a maximum entropy-based filter (32) on the mCFP channel. If one nucleus was present, we used a minimum filter on the CFP channel to locate the SPB. If no SPB was detected at this stage, we used the Intermodes (33) filter instead. For cells with two nuclei, we limited the region to find a SPB to the area around the nucleus. We used a Moments-based filter (34) to find each SPB. For cells with >2 nuclei, we repeated the nucleus count with a Moments-based filter and limited the SPB search to the two identified nuclei. If three nuclei remained, the cells were removed from analysis.

We used the two-dimensional position to determine which slice contained the center of each SPB so that only seven slices would be counted in the quantitation.

We removed from our final data sets any SPBs not detected in the full seven slices of fluorescence, any cells with more than three detected SPBs, or any SPBs located within 22 pixels of another SPB. We measured autofluorescence and bleedthrough in cells expressing only mCFP segmentation proteins without a quantitative mYFP protein to obtain measurements of the baseline global and local fluorescence noise. We removed measurements within one standard deviation of this baseline noise.

RESULTS

Interactions among ligands Sid2p and Mob1p and receptor Cdc11p

We defined the potential reactions of species visible by microscopy between the kinase Sid2p (S), its accessory protein Mob1p (M), and its SPB-bound receptor Cdc11p (R). The relevant bulk reactions are three:

$$\begin{aligned} S + M + R &\underset{K_{d,SMR}}{\rightleftharpoons} SMR, \\ 2 \cdot S + R &\underset{K_{d,SSR}}{\rightleftharpoons} S_2R, \\ 2 \cdot M + R &\underset{K_{d,MMR}}{\rightleftharpoons} M_2R. \end{aligned}$$

Because molecule counting was limited to the SPB, our method does not consider the reactions of the different ligands and receptors in the cytoplasm. Three reactions taking place exclusively in the cytoplasm are spectroscopically silent in our assay:

$$\begin{aligned} 2 \cdot S &\underset{K_{d,SS}}{\rightleftharpoons} S_2, \\ 2 \cdot M &\underset{K_{d,MM}}{\rightleftharpoons} M_2, \\ S + M &\underset{K_{d,SM}}{\rightleftharpoons} SM. \end{aligned}$$

We can detect the following species on the SPB: SR, MR, S_2R, M_2R, and SMR. The following potential stepwise interactions might contribute to binding of these species to the SPB:

$$\begin{aligned} SM + R &\underset{K_{d,SMR}}{\rightleftharpoons} SMR, \\ S + R &\underset{K_{d,SR}}{\rightleftharpoons} SR, \\ M + R &\underset{K_{d,MR}}{\rightleftharpoons} MR, \\ S + MR' &\underset{K_{d,SMR'}}{\rightleftharpoons} SMR, \\ S + SR'' &\underset{K_{d,SSR''}}{\rightleftharpoons} S_2R, \\ M + MR' &\underset{K_{d,MMR'}}{\rightleftharpoons} M_2R, \\ M + SR'' &\underset{K_{d,SMR''}}{\rightleftharpoons} SMR. \end{aligned}$$

Some of these species are indistinguishable in our assay, leaving the following reactions:

$$S + MR' \underset{K_{d,SMR'}}{\rightleftharpoons} SMR, \quad (1)$$

$$2 \cdot S + R \underset{K_{d,SSR}}{\rightleftharpoons} S_2R, \quad (2)$$

$$M + SR'' \underset{K_{d,SMR''}}{\rightleftharpoons} SMR, \quad (3)$$

$$2 \cdot M + R \underset{K_{d,MMR}}{\rightleftharpoons} M_2R. \quad (4)$$

In addition to free R Cdc11p, the three receptor species are MR′ with Mob1p bound, SR″ with Sid2p bound, and R with two ligand molecules bound. We determined $K_{d,SMR'}$ and $K_{d,SSR}$ by monitoring binding to the SPB over a range of concentrations of Sid2p and $K_{d,SMR''}$ and $K_{d,MMR}$ as we varied the concentration of Mob1p in the cell. The shapes of the binding curves depended on the order of the reaction.

Mitotic cells may contain phosphorylated heterodimers of Sid2p-Mob1p that bind SPBs but also translocate to the contractile ring (16). The reaction at the SPB is

$$SpM + R \underset{K_{d,SpMR}}{\rightleftharpoons} SpMR. \quad (5)$$

Construction of strains for medium throughput quantitative microscopy

Our objective was to measure the affinities of signaling proteins for SPBs of live fission yeast cells across the cell cycle. We tagged the ligand proteins with mYFP at their N-termini in their endogenous chromosomal loci and varied the expression of the fusion protein using combinations of thiamine-repressible promoters, thiamine concentrations, and induction times (Fig. 1). All strains with mYFP-tagged ligands also expressed proteins tagged with mCFP to localize the nucleus and SPBs (Table S1). These mCFP tags colocalized with the mYFP-tagged SPB ligands, but the proteins tagged with mCFP were physically located far enough from the mYFP ligands on SPBs to avoid any FRET-based changes in intensity. We chose the SUN protein Sad1p to mark SPBs, because it is localized on the inner side of the nuclear envelope (35), whereas all three of our proteins of interest are located primarily on the cytoplasmic face of the SPB (11). Rather than using potentially toxic DNA dyes to locate nuclei in live cells, we labeled the nuclear membrane with the low abundance, nonessential nucleoporin Seh1p-mCFP. In addition to segmenting images by color, we used fluorescence intensity to segment multiple signals. The high intensity of 2x-mCFP attached to Sad1p allowed us to separate the signal of the segmented SPB from the less intense Seh1-mCFP on the nuclear envelope.

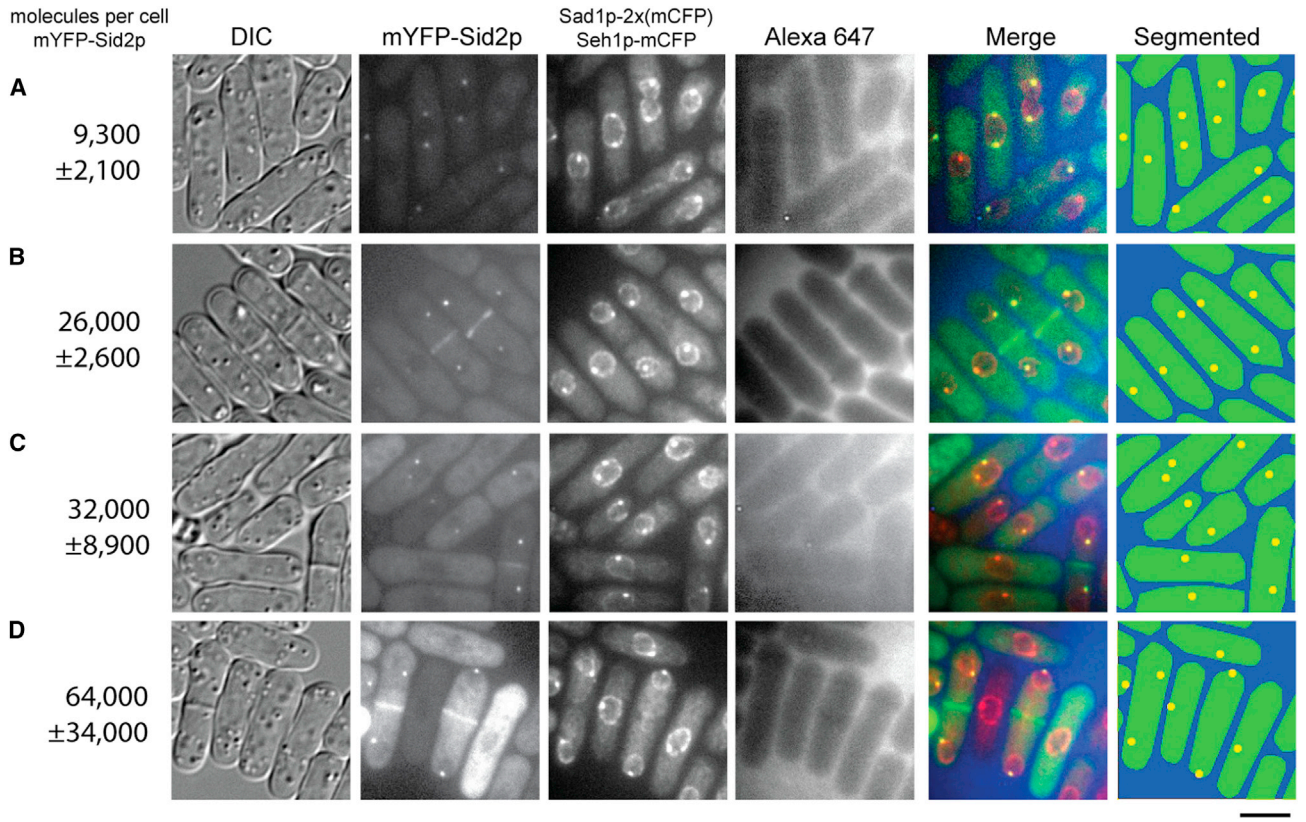

FIGURE 1 Contrast-independent segmentation of images of fission yeast cells expressing a range of concentrations of the SIN kinase Sid2p. (*A–D*) Cells expressed mYFP-Sid2p at a range of levels determined by the promoter and inducing conditions. These cells also expressed the nucleoporin Seh1p-mCFP to mark the nuclear envelope and Sad1p-2x(mCFP) to mark the SPB. The medium contained membrane-impermeant dye Alexa 647 to outline cells. The seven columns correspond (*L–R*) to 1), counts of mean numbers (±SD) of the total fluorescent mYFP-Sid2p molecules present in each cell of the selected field; (2), a DIC micrograph; 3), a sum projection fluorescent micrograph of the signal from mYFP-Sid2p; 4), a sum projection fluorescent micrograph of the signal from Seh1p-mCFP and Sad1p-2x(mCFP); 5), sum projection fluorescent micrograph of signal from Alexa 647 to outline cells; 6), a merged fluorescent micrograph showing (*green*) mYFP-Sid2p, (*red*) Sad1p-2x(mCFP), and Seh1-mCFP and (*blue*) Alexa 647; and 7), automatically segmented results showing individual cells in green and SPBs of any fluorescence intensity in yellow. Each row is one field of cells with the expression of Sid2p controlled by different promoters and inducing conditions: (*A*) the 41nmt1 promoter mYFP-Sid2p repressed by thiamine for 18 h; (*B*) WT mYFP-Sid2p under the control of the native promoter; (*C*) the 41nmt1 promoter induced by removing thiamine from growth media for 18 h; and (*D*) overexpression from the 3nmt1 promoter induced by removing thiamine from growth media for 18 h. Scale bar 5 μm.

Image acquisition and processing

We analyzed the binding reactions at defined points across the cell cycle to determine how they varied and to assure a homogeneous population of ligands and receptors in each sample. We used seven separate bins, four for interphase and three for mitosis (Fig. 2 *A*), similar to Salimova (18). We allocated cells to these bins based on a combination of criteria from DIC and sum projection fluorescent micrographs. Interphase bin I0 encompassed the G1, S, and early G2 phases of the cell cycle and contained fully septated cells that had yet to split into two daughter cells. We allocated interphase cells into three bins based on approximate volumes as determined by a ratio of area of the sum projection to the area of the average cell in relation to the average volume of 92 μm^3 determined by electron microscopy (8). Bin I1 included any cell below 80 μm^3, bin I2 had cells between 80 and 100 μm^3, and bin I3 included cells with volumes >100 μm^3 and only one apparent SPB. Mitotic bins included cells with two SPBs: bin M1, before anaphase B determined by the close proximity of the two SPBs; bin M2 from the onset of anaphase B with progressive separation of SPBs to a maximum; and bin M3, after maximum separation of SPBs and before completion of a septum. Cells with closely spaced SPBs were removed from bin M1.

A custom mCFP image-based segmentation in ImageJ automatically determined the three-dimensional positions and intensities of mYFP fluorescence associated with the 9 pixel wide, 7 pixel deep SPBs. Fluorescence intensities of mYFP were converted to numbers of mYFP-tagged molecules with calibration curves (Fig. S1), which agreed closely with alternative fluorescence-based methods (37,38) (Fig. S2). We converted these molecule counts to concentrations given the diffusive volume available in the relevant compartment of the cell (cytoplasm for Sid2p and Cdc11p; cytoplasm and nucleus for Mob1p) (25).

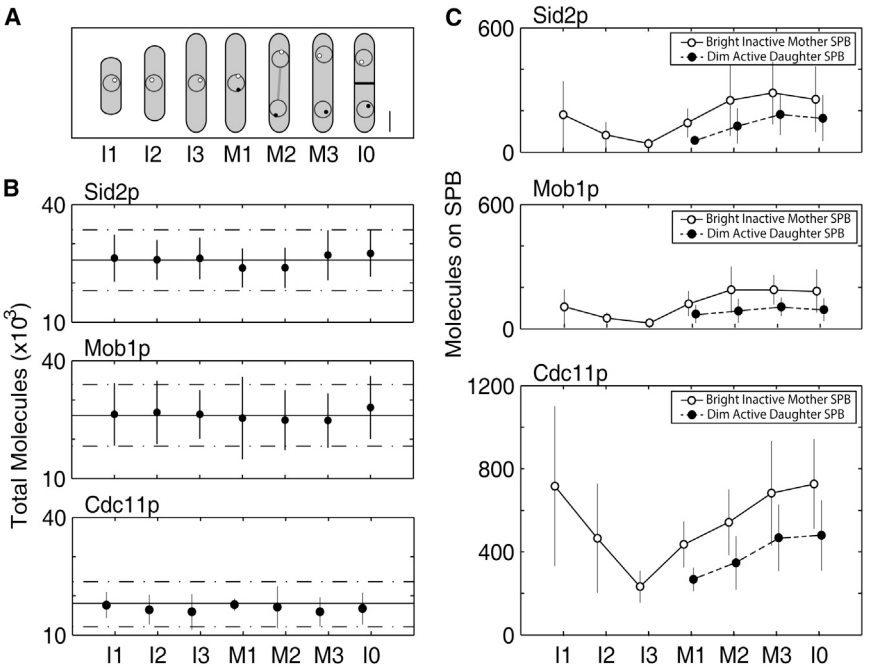

FIGURE 2 Measurements by quantitative fluorescence microscopy of total and local (SPB) numbers of cytokinesis proteins across the cell cycle. (*A*) Cartoon of *S. pombe* life cycle. Bin designations are based on cell volumes (average volume is 92 μm^3), the positions of SPBs and the presence of a complete septum from DIC images: (I1) interphase cells with apparent volume <80 μm^3; (I2) cells with volumes between 80 and 100 μm^3; (I3) interphase cells with volumes >100 μm^3 before SPB separation; (M1) anaphase A; (M2) anaphase B to maximum SPB separation; (M3) after maximum separation but before complete septum formation; and (I0) complete septum formation without cells splitting. Scale bar 5 μm. (*B*) Total numbers of molecules per cell (●) of SIN proteins (*top to bottom*) Sid2p, Mob1p, and Cdc11p throughout the cell cycle. Horizontal solid lines are average counts of total molecules across the cell cycle with $\pm 30\%$ error as dashed lines. (*C*) Absolute counts of molecules localized to the SPB with the same format as in (*B*). In cells with two SPBs (●) represent active dim SPBs and (○) represent inactive bright SPBs.

Measurement of SIN proteins associated with SPBs across the cell cycle

We used quantitative fluorescence microscopy to measure the numbers of molecules of three SIN proteins localized on the SPB of WT cells expressing mYFP-tagged versions of the proteins from their native loci (Fig. 1). The receptor is Cdc11p, and the two ligands are the kinase Sid2p and its accessory protein Mob1p. Although the total cellular counts of each protein were constant throughout the cell cycle (see Fig. 2 *B*), the local accumulation of each protein on SPBs fluctuated cyclically (see Fig. 2 *C*). The number of Cdc11p receptors associated with the SPBs always exceeded the numbers of ligands by at least a factor of two, indicating that the receptors were never saturated in WT cells.

Cell lines with Sid2p and Mob1p expressed at a range of levels

To measure the affinities of mYFP-Sid2p and mYFP-Mob1p for Cdc11p we varied the cellular concentrations of the two ligands using yeast strains with various inducible promoters. The *3nmt1* promoter strongly induced each protein, the *41nmt1* promoter recapitulated near WT expression levels, and the *81nmt1* promoter produced concentrations typically lower than WT cells. These promoters and the mYFP tag were placed in the endogenous loci of the *sid2+* and *mob1+* genes to ensure that every copy of the target protein was fluorescently tagged with mYFP and that cells in each microscopic field had a range of ligand expression. The resulting total cell concentrations of Sid2p and Mob1p ranged from barely detectable to over 25 μM, more than an order of magnitude over the WT expression levels (Fig. 1 and Fig. 2).

Abnormally elevated SIN activity, as in overexpression of either Sid2p or Mob1p, leads to activation of septation and initiation of mitosis in much smaller interphase cells than normal late G2 WT cells (4,40), therefore such cells divide prematurely and are smaller on average during interphase. We confirmed that cells with abnormally high or low concentrations of Sid2p or Mob1p are smaller than WT cells (Fig. S3 *C*). This alteration of cell size had no impact on our binning method during mitosis, because it relies on SPB positions and septation, but did alter the allocation of cells among the interphase bins, which are based on volumes. Consequently, our binning criteria misallocated many I3 cells into the I2 bin and many I2 and I3 cells into the I1 bin (Fig. S3, *D* and *E*), as explained in detail in the Supporting Material. We considered the altered compositions of these bins when interpreting the observations.

Approach for analysis of in vivo binding data

At all points in the cell cycle the numbers of ligand molecules associated with SPBs depended on the cytoplasmic concentration of free ligands, mYFP-Sid2p, and mYFP-Mob1p (Fig. 3, S5–S7). In all cases the numbers of ligands associated with a SPB increased with the cytoplasmic ligand concentration, but hyperbolic isotherms describing a simple bimolecular reaction did not fit the data well.

We developed a strategy to analyze this in vivo binding data based on our understanding of the reactants and possible products (16). We assumed that more than one

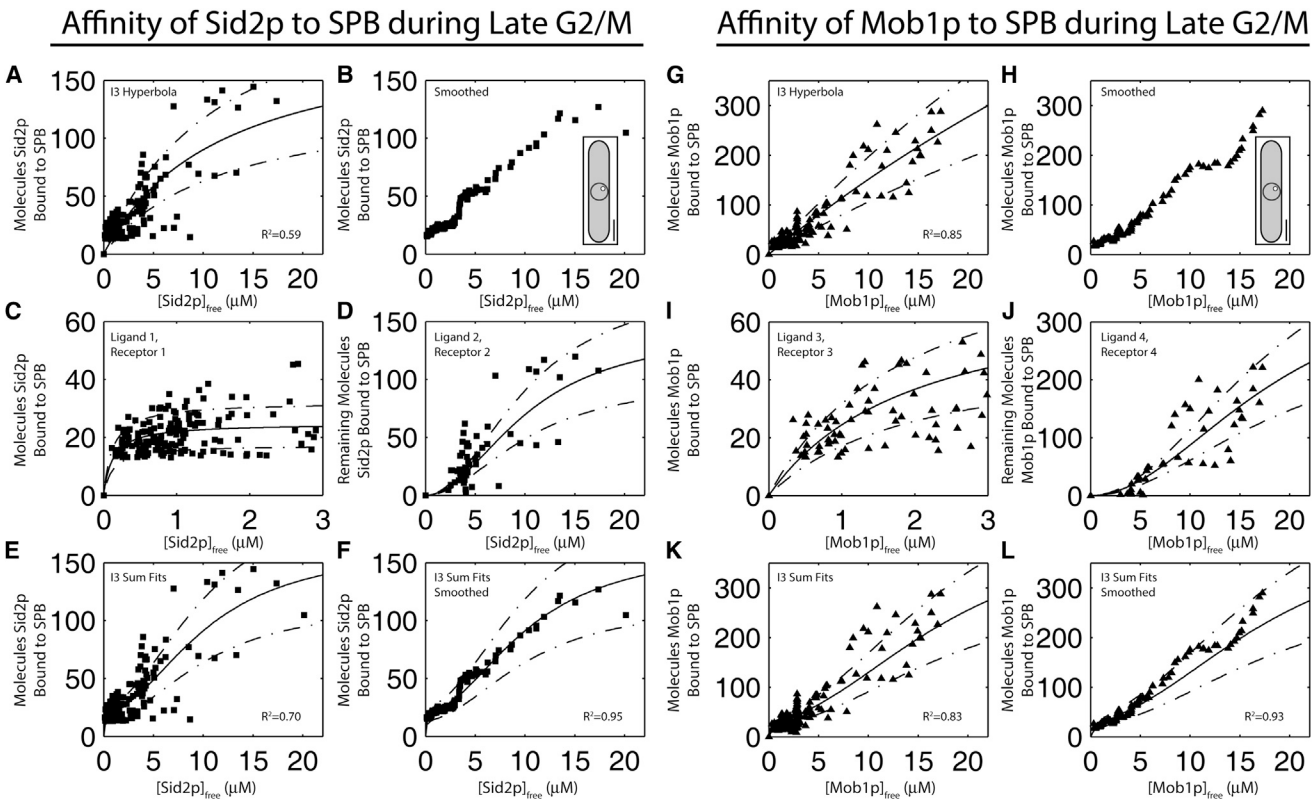

FIGURE 3 Affinity of (*A–F*) Sid2p and (*G–L*) Mob1p for the SPB in live interphase cells in volume bin I3 representing Late G2/M. (*A*) Dependence of the numbers of mYFP-Sid2p molecules associated with the SPB on the cytoplasmic concentration of mYFP-Sid2p in bin I3. A hyperbola representing a simple bimolecular reaction did not fit the data well. (*B*) Substructure in the data was revealed by smoothing with a robust local weighted regression (*rlowess*) using a span of the square root of number of cells measured. A nodal point at 3 μM Sid2p separates the reactions. (*Inset*) Cartoon of late G2/M cell. Scale bar 5 μm. (*C*) Hyperbolic fit to low concentrations of $[Sid2p]_{free}$ isolates an initial plateau for Reaction 1 in which Receptor 1 binds Ligand 1. (*D*) After subtracting the contribution of the reaction from the measurements cells expressing all concentrations of $[Sid2p]_{free}$, the residual data have a sigmoidal shape that can be fit with a Hill equation assuming cooperativity or multimer Sid2p binding. We define this as Reaction 2 with Ligand 2 binding to Receptor 2. (*E*) The fit of the sum of a hyperbola and sigmoid, done exclusively with raw data. (*F*) Same fit superimposed on smoothed data to evaluate the goodness of fit. R^2 is 0.95. (*G–L*) Affinity of mYFP-Mob1p for the SPB in live cells during interphase. The data for cells expressing a range of mYFP-Mob1p concentrations were analyzed using the same procedures used for Sid2p (*panels A–F*).

binding reaction contributes to the ligands associated with SPBs and recognized that Sid2p and Mob1p not only compete for binding the Cdc11p receptors but also bind receptors as monomers, homodimers, and heterodimers. Considering all of these reactions allowed us to account for all of the receptors and to identify the most likely ligands. The analysis also revealed the existence of two species of receptors, type 1 and type 2, at all points in the cell cycle. Fortunately, the two forms of Cdc11p receptors generally bind the ligands with very different affinities, allowing us to distinguish the two classes of receptors over a wide range of ligand concentrations.

We began our analysis with cells in interphase bin I3, where Sid2p and Mob1p binding are relatively straightforward compared with mitotic cells containing phosphorylated Sid2p-Mob1p heterodimers. The numbers of mYFP-Sid2p or mYFP-Mob1p bound to SPBs increased with the concentrations of each free ligand up to nearly 150 molecules of Sid2p per SPB (Fig. 3 *A*) and nearly 300 molecules of mYFP-Mob1p per SPB (see Fig. 3 *G*). However, hyperbolas corresponding to the reaction ligand + Cdc11p $\rightleftharpoons$ ligand-Cdc11p did not fit the data well for either Sid2p or Mob1p, so simple 1:1 binding of these ligands to a homogeneous population of receptors do not explain the data.

Smoothing the data with an algorithm to reduce the noise inherent in our measurements (Fig. 3, *B* and *H*), revealed substructure in the I3 data with the appearance of apparent plateaus at low concentrations of either ligand followed by further binding at higher ligand concentrations.

We used an iterative process to analyze the binding of Sid2p and Mob1p. After making an approximate fit to the high-affinity data at low concentrations of free ligand, we subtracted this binding isotherm from the entire data set to reveal the low-affinity data. Fits to the low-affinity data were then used to remove the low-affinity signal from the high-affinity data. This approach to fitting a combination

of two binding reactions (41) is more effective than a general least squares minimization over the entire set of data. The combined analysis of both data sets allowed us to propose the identity of each ligand and receptor species and to account for the stoichiometry.

Analysis of Sid2p binding during interphase

The dependence of Sid2p binding to SPBs on ligand concentration had a clear plateau well below the maximum number of Sid2p capable of binding the SPB. We considered two hypotheses to explain this intermediate plateau, two species of ligand or two species of receptors. Simple models showed that a mixture of two species of ligand with different affinities for a homogeneous pool of Cdc11p receptors would give a smooth curve with half-maximal saturation between the two K_ds. On the other hand, the presence of two classes of Cdc11p receptors with different affinities for the ligand is consistent with the presence of an apparent plateau at intermediate concentrations of ligand. In this particular case, the data suggested a small subset of receptors binding mYFP-Sid2p with high affinity and a larger number of Cdc11p molecules binding mYFP-Sid2p with much lower affinity (Fig. 3, *A–F*).

We started the fit of the Sid2p data at free ligand concentrations <3 μM. A simple hyperbola fit the numbers of mYFP-Sid2p bound to the SPB at low cytoplasmic concentrations of mYFP-Sid2p (Fig. 3 *C*), as expected for a simple bimolecular reaction. For presentation purposes, we define this as Reaction 1 between Ligand 1 and Receptor 1. The K_d for Reaction 1 is <0.1 μM with 25 Sid2p molecules saturating Receptor 1 on the plateau. After removing the small contribution of Reaction 2 from the total data (see below), the plateau for Reaction 1 was 22 molecules Sid2p bound to Receptor 1 with an affinity <0.1 μM. This subset of receptors is far below the 236 molecules of Cdc11p associated with the SPB at this stage of the cell cycle (Fig. 2 *C*). From our reaction schemes, Ligand 1 might be a mYFP-Sid2p monomer, homodimer, or heterodimer with Mob1p. The numbers of Receptor 1 sites were close to the numbers of Mob1p bound to the SPB in WT cells in bin I3.

At cytoplasmic mYFP-Sid2p concentrations >3 μM larger numbers of mYFP-Sid2p bound to SPBs, but given the absence of a clear plateau, the affinity must be low (Fig. 3 *D*). We call this low-affinity subspecies of Cdc11p Receptor 2. To analyze these data, we removed the contribution of mYFP-Sid2p bound to the high-affinity site at all concentrations of mYFP-Sid2p by subtracting the Reaction 1 binding curve from all of the data points. At high concentrations of mYFP-Sid2p the numbers of molecules bound to SPBs had a sigmoidal distribution suggesting that Reaction 2 involves either a homodimeric $(Sid2p)_2$ ligand, cooperative binding, or some combination of the two.

We explored the lack of a robust plateau at high concentrations of free Sid2p by testing several hypotheses. The simplest is that the highest Sid2p concentration tested did not saturate all available receptor sites. Alternatively, some biochemical mechanism might prevent some receptors from binding Sid2p. We tested the first hypothesis by assuming that all of Cdc11p is active, considered three different stoichiometries, and attempted to fit the data (Fig. S4). We tested Sid2p monomers and homodimers as the ligand or did not constrain the stoichiometry, allowing a fraction of the Cdc11p to bind Sid2p monomers or homodimers. The unconstrained mechanism fit the smoothed data better than the mechanism with monomeric or homodimeric Sid2p as the ligand. The best fit of the Hill equation had a cooperativity of 2 with 143 molecules of Receptor 2 and half-maximal saturation at ~10.2 μM mYFP-Sid2p. This corresponds to an affinity of 106 μM (Fig S4, *E* and *F*). Thus, we favor the hypothesis that only a subset of Cdc11p is available for binding to either monomers or homodimers in this stage of the cell cycle.

The fits to the I2 bin revealed that the affinities of mYFP-Sid2p for Receptor 1 and Receptor 2 were nearly identical to the affinities measured in cells in the I3 bin, although the numbers of bound ligand on each plateau were higher because of the larger number of Cdc11p receptors (Fig. S5, *A–E*).

Analysis of Mob1p binding during interphase

We measured binding of mYFP-Mob1p to SPBs of cells in bin I3 over a wide range of free mYFP-Mob1p concentrations (Fig. 3 *G*). The distribution of data points was similar to the experiments with mYFP-Sid2p, so we used the same strategy to analyze the Mob1p data.

We first considered high-affinity binding of mYFP-Mob1p to SPBs. We defined this as Ligand 3 binding Receptor 3. A simple hyperbolic curve fit well to the data in cells with <3 μM mYFP-Mob1p (Fig. 3 *I*). After subtracting the signal for low-affinity binding at mYFP-Mob1p concentrations >3 μM, the fit to the high-affinity data gave a K_d of 1.0 μM for mYFP-Mob1p binding to 47 $\pm$ 8 molecules of Receptor 3, similar to the numbers (36 $\pm$ 25) of the potential receptor Sid2p-Cdc11p.

We analyzed the low-affinity binding of mYFP-Mob1p to SPBs using the cells expressing >3 μM free Mob1p. After we removed the contribution of the high-affinity hyperbolic binding reaction from the total mYFP-Mob1p binding data, these data were sigmoidal (Fig. 3 *J*). The low-affinity data lacked a robust plateau, therefore we first assumed all Cdc11p are available for binding Mob1p homodimers. Unlike the Sid2p data, this assumption provided us with an excellent fit. We defined this as Ligand 4 binding Receptor 4. The Hill equation with $n = 2$ and a plateau of 400 binding sites fit the data well. This number contrasts with Sid2p, which did not saturate the 236 available Cdc11p molecules. These values correspond to an apparent affinity of 358 μM (Fig. 3 *L*), equivalent to an EC_{50} value of

19 μM. Given the sigmoidal nature of the curve we assume this ligand to be equilibrium between monomeric Mob1p and homodimers.

Fits to the I2 bin of the mYFP-Mob1p experiment yielded affinities similar to the I3 bin only with higher plateau values as more Cdc11p associates with SPBs in the middle of interphase (Fig. S5, *F–J*).

Analysis of Sid2p and Moblp binding during mitosis

We analyzed Sid2p binding to the two SPBs in mitotic cells separately (Fig. S6). Compared with mother SPBs, the dim daughter SPBs had lower mYFP-Sid2p fluorescence signals and more Cdc7p kinase to phosphorylate the Sid2p/Mob1p heterodimer (10) (Fig. S8). The smoothed data for mitotic bin M1 (Fig. S6, *B* and *H*), showed clear high- and low-affinity regions, so we analyzed the mitotic data with the same strategy used for interphase data with high-affinity Receptor 1 and the low-affinity Receptor 2. We separated the data into two halves around 3 μM, fit the tight binding reaction at low ligand concentrations to a hyperbola, removed the hyperbola's influence from all of the data, fit the weak binding reaction to the Hill equation, and adjusted the hyperbola for the contribution of the Hill equation.

For the cells in mitotic bin M1 the dependence of mYFP-Sid2p binding to SPBs on ligand concentration was similar for the bright and dim SPBs. Although the data were noisy, the fits clearly indicated that mYFP-Sid2p bound Receptor 1 on both SPBs with lower affinities than during interphase (Fig. S6 *A*). Additionally, at low concentrations of free mYFP-Sid2p, the numbers of mYFP-Sid2p associated with SPBs were generally higher than the numbers of the presumed receptor Mob1p-Cdc11p at SPBs in WT cells (see Fig. 2, *B* and *C*, and Fig. S6, *E* and *M*).

Our measurements showed that Sid2p-Mob1p heterodimers have lower affinity for Receptor 1 on the SPB during mitosis than interphase, whereas Sid2p homodimers have higher apparent affinities for low-affinity Receptor 2 during mitosis. Consequently, ignoring the potential role of cooperativity in the reactions and just looking at the EC_{50}, the ligand concentration that saturates half of the receptor species, the two affinities differed by less than an order of magnitude at some points in mitosis (see Fig. 4 *B*), making it more difficult to parse the contributions of each reaction.

At high cytoplasmic concentrations the numbers of mYFP-Sid2p associated with SPBs of cells in bin M1 exceeded the numbers of total Cdc11p receptors by about a factor of two (Fig. S6, *A*, *B*, *G*, and *H*). This suggested that Receptor 2 was fully saturated with homodimers of mYFP-Sid2p. Fig. S7 also shows the analysis of mYFP-Sid2p binding to SPBs at other stages of mitosis and mYFP-Mob1p binding to mitotic SPBs.

DISCUSSION

Our analysis revealed that binding of the SIN kinase Sid2p to SPBs is not a simple bimolecular reaction, and we predict that analysis of other binding reactions under physiological conditions will also reveal complexity not apparent in biochemical assays. We found that SPBs bind both Sid2p-Mob1p heterodimers and Sid2p homodimers, but during interphase the affinity for heterodimers is stronger by two orders of magnitude (Fig. 4 *B*). During mitosis SPBs have similar EC50s for the two ligands.

Measuring affinities in live cells by counting molecules

Our proof of principle experiments with SPBs binding Sid2p and Mob1p show that one can measure binding by quantitative fluorescence microscopy in live cells and with a basic understanding of the molecular mechanism calculate thermodynamic parameters for the system throughout the cell cycle. We establish that this approach can measure K_ds ranging from hundreds of nanomolar to tens of micromolar and possibly higher if cooperativity is involved.

The analysis depended on being able to replace the endogenous copies of proteins of interest with fluorescent copies and to vary the concentrations of both free ligands independently over a wide range. The analysis also depended on a reliable method to measure the number of molecules locally and globally in cells (8) coupled with a semiautomatic method to acquire data sets two orders of magnitude larger than manual methods. The spinning disk confocal microscope provided high spatial resolution, sensitivity, and wide dynamic range.

We compared our method to count molecules with alternative methods using an internal standard (37,38) and found agreement to within 30% of our absolute numbers (Fig. S2). Other laboratories are debating the best standards to calibrate fluorescent microscopes for counting molecules (42–44), so the absolute numbers may have to be adjusted in the future. If our numbers were off by a factor of two, the affinities would be adjusted in direct proportion. This difference would be small compared to the order of magnitude difference between the strong binding of heterodimers and the weak binding of homodimers to the SPB.

Analysis of binding data during interphase

The shapes of the binding curves for the Sid2p and Mob1p revealed two receptor states. A limited number of Cdc11p receptors have a high affinity for heterodimers. We refer to these as type 1 receptors. A larger number of low-affinity receptors bind homodimers cooperatively at high concentrations of ligand. We refer to these as type 2 receptors. Our analysis indicates that type 1 receptors participate

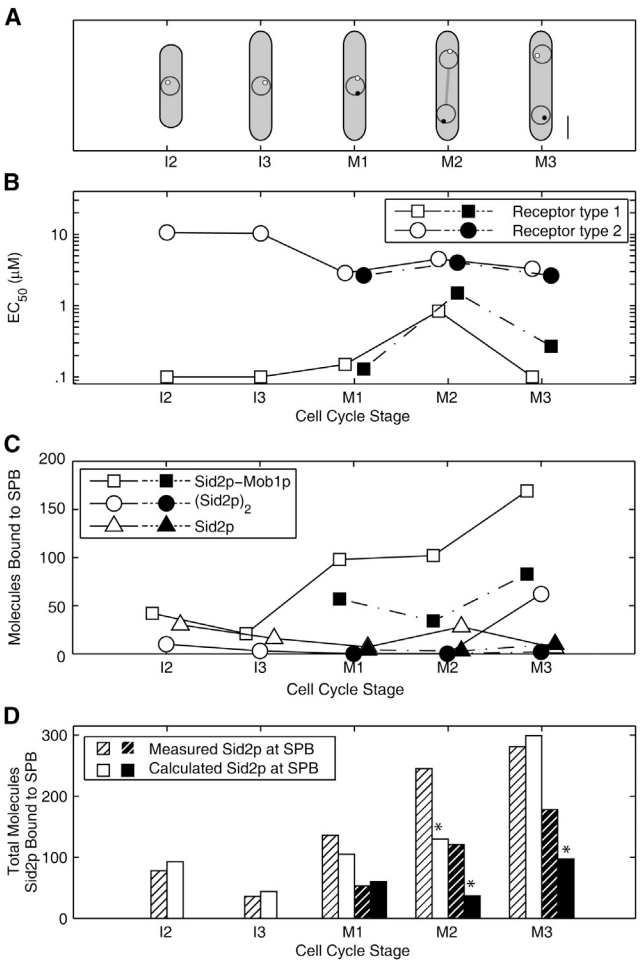

FIGURE 4 Changes in the affinity of Sid2p for the SPB across the cell cycle reveals a cycle of high- and low-affinity states that can be used to calculate the number of species present on SPB throughout the cell cycle. (*A*) Cartoon of portions of *S. pombe* life cycle from which affinity measurements were derived. Scale bar 5 μm. (*B*) Log plot of the EC50 (μM) measured from (□, ■) the low concentrations of Sid2p that bind receptor type 1, and (○, ●) the high concentrations of Sid2p that bind receptor type 2 throughout the cell cycle. The cells in bins I0 and I1 were mixtures of cells at different cell cycle stages, so they could not be analyzed. (*C*) Plot of distribution of Sid2p under WT conditions at the SPB throughout the cell cycle. Calculated species of (□, ■) total heterodimer, (○, ●) Sid2p homodimer, and (△, ▲) monomer bound to the SPB in each cell cycle bin given the WT concentrations of Sid2p and Mob1p in the cell, the total Mob1p and Cdc11p bound to the SPB, and determined affinities from (*B*) and Table S2. Evaluating the affinity of Sid2p for type 1 receptors given the total number of Mob1p bound to the SPB in WT cells provides the Mob1p monomer bound and heterodimer bound, evaluating the affinity of Mob1p for type 1 receptors given the total number of heterodimer bound provides the Sid2p monomer bound, and evaluating the affinity of Sid2p for type 2 receptors given the total number of Cdc11p receptors in WT cells and the calculated occupied receptors from monomeric and heterodimeric bound species gives the number of Sid2p homodimers bound. Bound Sid2p was left out of the calculations so that it could be used to determine efficacy of our method. (*D*) Comparison of deriving bound Sid2p from free concentrations and affinities with measuring Sid2p bound to SPB throughout the cell cycle in WT cells. (*Striped bars*) Measured WT Sid2p bound to SPB as in Fig. 2 *C* top panel. (*Solid bars*) Summation of bound heterodimer, twice the bound homodimers, and bound Sid2p monomer from part (*C*). Solid symbols and bars represent dim active daughter SPBs. Open symbols and bars represent bright inactive mother SPBs. Asterisks indicate low estimation of bound Sid2p from calculations.

in Reactions 1 and 3 and type 2 receptors participate in Reactions 2 and 4.

We do not know how type 1 Cdc11p receptors differ from type 2 receptors. The type 1 subset of the Cdc11p may have a posttranslational modification giving a high affinity for Sid2p-Mob1p heterodimers. It seems less likely that SPBs have a high-affinity receptor other than Cdc11p (6,12).

Taking into account previous genetic and biochemical work (16) we identified both the ligand and receptor species for the four reactions in late interphase cells in bin I3 by considering both the Sid2p and Mob1p data. We propose that Ligand 1 is the Sid2p monomer, which binds with high affinity to a subset of only 22 molecules of Mob1p-Cdc11p, Receptor 1. Thus, the bound species is the heterodimer (Eq. 1) described by Reaction 1 and $K_{d,SMR'}$. Ligand 3 is likely the Mob1p monomer, which binds to Receptor 3, a type 1 receptor. Because low concentrations of Mob1p saturate Receptor 3 at the number of Sid2p bound to the SPB in WT interphase cells (47 molecules), we suggest that Sid2p-Cdc11p is Receptor 3 for Mob1p as described by Reaction 3 and $K_{d,SMR''}$.

Thus, the plateaus observed for high-affinity binding of both Sid2p and Mob1p to SPBs were similar to the number of molecules of the reciprocal ligand observed on SPBs in WT cells. Therefore, we favor the hypothesis that the receptors for Reactions 1 and 3 are Cdc11p with the partner ligand prebound, i.e., Mob1p-Cdc11p or Sid2p-Cdc11p. Although we could not measure the affinities of reactions in the cytoplasm, Sid2p-Mob1p heterodimers are likely to exist in the cytoplasm and contribute to binding to a limited number of Cdc11p sites on the SPB.

The ligands for Reaction 2 are likely to be a mixture of Sid2p monomers and homodimers that bind with low affinity to type 2 Cdc11p receptors (Eq. 2). The highest concentration of Sid2p tested saturated only half of the type 2 Cdc11p receptors during interphase (Fig. 2, *D* and *J*), but all of the receptors during mitosis (Fig. S6). The simplest explanation is that the affinity of type 2 receptors for Sid2p is >25 μM during interphase. Because the highest concentration of Sid2p tested did not saturate the receptors during interphase, some fraction of Cdc11p may be inactive. On the other hand, high concentrations of Mob1p occupy the type 2 Cdc11p receptors with a stoichiometry of >1 Mob1p per Cdc11p but with very low affinity, so whatever limits the saturation of the receptor by Sid2p may not apply to Mob1p. Ligand 4 is likely to be a mixture of monomers and Mob1p. Mob1p homodimers were previously ignored as a Cdc11p ligand, but *Saccharomyces cerevisiae* Mob1p forms dimers at high concentrations in solution and in crystals (19). WT concentrations of Mob1p allow very few if any Mob1p homodimers to bind SPBs because of their low affinity.

Changes in the affinities of SPBs for Sid2p and Mob1p during the cell cycle

Our main finding is that the affinities of SPBs for Sid2p-Mob1p heterodimers and Sid2p homodimers change reciprocally during the transitions into and out of mitosis (Fig. 4 *B*). Interphase conditions favor strong binding of Sid2p-Mob1p heterodimers to SPBs, whereas during mitosis SPBs bind both heterodimers and Sid2p homodimers with intermediate apparent affinities. These changes in affinity explain the fluctuations in the numbers of ligands bound to SPBs across the cell cycle (Fig. 2 *C* and Fig. 4 *C*).

Phosphorylation most likely contributes to the lower affinity of heterodimers for SPBs (Reactions 1 and 3) during mitosis (16) (Fig. 4 *B*), although we cannot rule out parallel changes in the type 1 and 2 receptors.

Explanation of the numbers of Sid2p and Mob1p on SPBs across the cell cycle

Although the total numbers of Cdc11p, Sid2p, and Mob1p in the cells do not fluctuate across the cell cycle (Fig. 2 *B*), the numbers of all three proteins associated with SPBs vary considerably depending on the stage of the cell cycle (Fig. 2 *C*). The number of Cdc11p receptors on SPBs peaks during mitosis and declines throughout interphase to reach a nadir just before the end of G2. During mitosis the numbers of Cdc11p on SPBs increases to a higher level on the inactive, bright SPB than the dim SPB. We have not studied the mechanism of this fluctuation in receptor number.

Our quantitative approach allowed us to calculate the numbers of Sid2p bound to SPBs across the cell cycle using the affinities of Reactions 1–4, the measured concentrations of ligands in WT cells and the numbers of Mob1p and Cdc11p bound to the SPBs (Fig. 4 *C*). We compared these calculated numbers of Sid2p with measured numbers bound to the SPB (Fig. 4 *D*). This calculation also gave us estimates of the various species of Sid2p bound to the SPBs.

The calculated occupancy of the SPBs during interphase, in mitosis before Anaphase B, and on bright inactive mitotic SPBs after maximum SPB separation agreed with numbers of Sid2p bound to SPBs in the WT cells within 22% (Fig. 4 *D*). These calculations underestimated by about a factor of two the numbers of Sid2p bound to the SPB during Anaphase B and to the active SPB after maximum SPB separation. Nevertheless, this agreement is remarkably good given the challenges in measuring some of the affinities in live cells. The poorest prediction during late anaphase may come from limitations in accounting for phosphorylated Sid2p, because we were unable to deconvolve that reaction from our data.

We conclude from our calculations that at least two factors control the numbers of Sid2p and Mob1p at the SPB. The dominant factor is the number of Cdc11p receptors on the SPB during the cell cycle. The cyclical nature of Cdc11p localization accounts for much of the cyclical variation of Sid2p and Mob1p numbers on the SPB. The other aspect not previously recognized is the influence of affinities on the association of ligands with the SPB. The ratio of Sid2p/Cdc11p fluctuates during the cell cycle due to variable affinities of heterodimers, monomers, and homodimers for the SPB (Fig. 4, *B* and *C*). As a result of its high affinity, the Sid2p-Mob1p heterodimer is the main species of Sid2p bound to the SPB throughout the cell cycle (Fig. 4 *C*).

Our quantitative analysis of Sid2p and Mob1p binding the SPB revealed the intricacies of binding in the cellular milieu. We verified the presence of Sid2p homodimers on SPBs in interphase and in mitosis in WT cells, especially on the inactive mother SPB where more homodimer binds than Sid2p monomers (Fig. 4 *C*). The higher affinity of type 2 Cdc11p receptors on mitotic SPBs for Sid2p homodimers results in binding of Sid2p and Mob1p homodimers (Table S3), which may compete with heterodimers as suggested (16). Previous work showed that heterodimers of Sid2p-Mob1p persist throughout the cell cycle, but it was unclear if these heterodimers were restricted to the cytoplasm or also associated with SPBs (16). We show that ~10% of Cdc11p receptors on SPBs of WT cells are occupied with heterodimers in interphase, but the fraction of these type 1 receptors occupied by heterodimers doubles during mitosis.

Early in mitosis the bright and dim SPBs differ in the number of receptors but those receptors have similar affinities for ligands. Given the role of active Sid2p-Mob1p in phosphorylating Cdc11p (12), it would not be surprising if active Sid2p-Mob1p on SPBs were to phosphorylate proteins that control the asymmetry of the SPB during mitosis and other substrates such as MOR pathway proteins (12,15). Phosphorylated heterodimers also dissociate to act on cytosolic targets such as Clp1p (13) and the contractile ring.

Previous approaches may have missed subtle differences in the occupancy of the two SPBs (Fig. S8). No evidence from our studies indicates that N-terminal tags on mYFP-Sid2p and mYFP-Mob1p compromise their function. The localization patterns of both proteins were similar, so mYFP-Sid2p is potentially more active than the C-terminally tagged Sid2p-GFP used in early studies (11). The main species of Sid2p bound to SPBs during interphase are monomers, homodimers, and heterodimers, all with characteristics that make visualization challenging in fixed cells. For example, immunofluorescence microscopy with an antibody specific for the N-terminal 205 residues of Sid2p did not detect Sid2p at interphase SPBs (14), whereas we counted a minimum of ~40 molecules of Sid2p on the SPB at this time. Perhaps weakly bound Sid2p monomers and dimers dissociate from the SPBs during fixation or the interaction of the N-terminal region of Sid2p with Cdc11p interfered with antibody binding.

CONCLUSIONS

We show that the technology exists to determine protein-protein interactions in their native environment. By increasing the throughput of the technique we were able to analyze reasonable numbers of cells and draw conclusions about changes in affinities throughout the cell cycle. Targets for future study by this method include proteins that bind to receptors associated with a microscopically distinct cellular structure and that are hard to purify or regulated by post-translational modifications.

We found that fission yeast Sid2p, the homolog of human tumor suppressor protein LATS1 (45), binds with high affinity to Cdc11p on the SPB with its activating protein Mob1p. This SPB recruitment facilitates phosphorylation and activation of the heterodimer. In addition, we show that the formation of kinase homodimers can sequester Sid2p from making heterodimers to inhibit premature signaling to start constriction of the medial actomyosin contractile ring.

SUPPORTING MATERIAL

Three tables, eight figures, Reference (46) and supporting methods and results are available at http://www.biophysj.org/biophysj/supplemental/S0006-3495(13)00930-2.

We thank Jian Qiu Wu, Julien Berro, Qian Chen, and Shalini Nag for helpful discussions and Ezra Baraban and Shambaditya Saha for help with experiments.

This work was supported by a National Institutes of Health research grant (GM026132) and a National Science Foundation Predoctoral Fellowship supporting C.M.

REFERENCES

1. Pollard, T. D. 2010. A guide to simple and informative binding assays. *Mol. Biol. Cell.* 21:4061–4067.
2. Simanis, V. 2003. The mitotic exit and septation initiation networks. *J. Cell Sci.* 116:4261–4262.
3. Krapp, A., M. P. Gulli, and V. Simanis. 2004. SIN and the art of splitting the fission yeast cell. *Curr. Biol.* 14:R722–R730.
4. Csikász-Nagy, A., O. Kapuy, …, B. Novák. 2007. Modeling the septation initiation network (SIN) in fission yeast cells. *Curr. Genet.* 51:245–255.
5. Krapp, A., and V. Simanis. 2008. An overview of the fission yeast septation initiation network (SIN). *Biochem. Soc. Trans.* 36:411–415.
6. Morrell, J. L., G. C. Tomlin, …, K. L. Gould. 2004. Sid4p-Cdc11p assembles the septation initiation network and its regulators at the *S. pombe* SPB. *Curr. Biol.* 14:579–584.
7. Krapp, A., S. Schmidt, …, V. Simanis. 2001. *S. pombe* cdc11p, together with sid4p, provides an anchor for septation initiation network proteins on the spindle pole body. *Curr. Biol.* 11:1559–1568.
8. Wu, J. Q., and T. D. Pollard. 2005. Counting cytokinesis proteins globally and locally in fission yeast. *Science.* 310:310–314.
9. Magidson, V., F. Chang, and A. Khodjakov. 2006. Regulation of cytokinesis by spindle-pole bodies. *Nat. Cell Biol.* 8:891–893.
10. Grallert, A., A. Krapp, …, I. M. Hagan. 2004. Recruitment of NIMA kinase shows that maturation of the *S. pombe* spindle-pole body occurs over consecutive cell cycles and reveals a role for NIMA in modulating SIN activity. *Genes Dev.* 18:1007–1021.
11. Sparks, C. A., M. Morphew, and D. McCollum. 1999. Sid2p, a spindle pole body kinase that regulates the onset of cytokinesis. *J. Cell Biol.* 146:777–790.
12. Feoktistova, A., J. Morrell-Falvey, …, K. L. Gould. 2012. The fission yeast septation initiation network (SIN) kinase, Sid2, is required for SIN asymmetry and regulates the SIN scaffold, Cdc11. *Mol. Biol. Cell.* 23:1636–1645.
13. Chen, C. T., A. Feoktistova, …, D. McCollum. 2008. The SIN kinase Sid2 regulates cytoplasmic retention of the *S. pombe* Cdc14-like phosphatase Clp1. *Curr. Biol.* 18:1594–1599.
14. Grallert, A., Y. Connolly, …, I. M. Hagan. 2012. The *S. pombe* cytokinesis NDR kinase Sid2 activates Fin1 NIMA kinase to control mitotic commitment through Pom1/Wee1. *Nat. Cell Biol.* 14:738–745.
15. Gupta, S., S. Mana-Capelli, …, D. McCollum. 2013. Identification of SIN pathway targets reveals mechanisms of crosstalk between NDR kinase pathways. *Curr. Biol.* 23:333–338.
16. Hou, M. C., D. A. Guertin, and D. McCollum. 2004. Initiation of cytokinesis is controlled through multiple modes of regulation of the Sid2p-Mob1p kinase complex. *Mol. Cell. Biol.* 24:3262–3276.
17. Hou, M. C., J. Salek, and D. McCollum. 2000. Mob1p interacts with the Sid2p kinase and is required for cytokinesis in fission yeast. *Curr. Biol.* 10:619–622.
18. Salimova, E., M. Sohrmann, …, V. Simanis. 2000. The *S. pombe* orthologue of the *S. cerevisiae* mob1 gene is essential and functions in signalling the onset of septum formation. *J. Cell Sci.* 113:1695–1704.
19. Mrkobrada, S., L. Boucher, …, F. Sicheri. 2006. Structural and functional analysis of *Saccharomyces cerevisiae* Mob1. *J. Mol. Biol.* 362:430–440.
20. Hoppe, A. D., S. L. Shorte, …, R. Heintzmann. 2008. Three-dimensional FRET reconstruction microscopy for analysis of dynamic molecular interactions in live cells. *Biophys. J.* 95:400–418.
21. Sudhaharan, T., P. Liu, …, S. Ahmed. 2009. Determination of in vivo dissociation constant, KD, of Cdc42-effector complexes in live mammalian cells using single wavelength fluorescence cross-correlation spectroscopy. *J. Biol. Chem.* 284:13602–13609.
22. Shi, X., Y. H. Foo, …, T. Wohland. 2009. Determination of dissociation constants in living zebrafish embryos with single wavelength fluorescence cross-correlation spectroscopy. *Biophys. J.* 97:678–686.
23. Winter, P. W., J. T. McPhee, …, B. G. Barisas. 2011. Fluorescence correlation spectroscopic examination of insulin and insulin-like growth factor 1 binding to live cells. *Biophys. Chem.* 159:303–310.
24. Slaughter, B. D., J. W. Schwartz, and R. Li. 2007. Mapping dynamic protein interactions in MAP kinase signaling using live-cell fluorescence fluctuation spectroscopy and imaging. *Proc. Natl. Acad. Sci. USA.* 104:20320–20325.
25. Wu, J. Q., C. D. McCormick, and T. D. Pollard. 2008. Chapter 9: Counting proteins in living cells by quantitative fluorescence microscopy with internal standards. *Methods Cell Biol.* 89:253–273.
26. Pollard, T. D., and J. Q. Wu. 2010. Understanding cytokinesis: lessons from fission yeast. *Nat. Rev. Mol. Cell Biol.* 11:149–155.
27. Coffman, V. C., and J. Q. Wu. 2012. Counting protein molecules using quantitative fluorescence microscopy. *Trends Biochem. Sci.* 37:499–506.
28. Bähler, J., J. Q. Wu, …, J. R. Pringle. 1998. Heterologous modules for efficient and versatile PCR-based gene targeting in *Schizosaccharomyces pombe*. *Yeast.* 14:943–951.
29. Hentges, P., B. Van Driessche, …, A. M. Carr. 2005. Three novel antibiotic marker cassettes for gene disruption and marker switching in *Schizosaccharomyces pombe*. *Yeast.* 22:1013–1019.
30. Ti, S.-C., C. Jurgenson, …, T. D. Pollard. 2011. Structural and biochemical characterization of two binding sites for nucleation promoting factor WASp-VCA on Arp2/3 complex. *Proc. Natl. Acad. Sci. USA.* 108:E463–E471.

31. Meijering, E. H., W. J. Niessen, and M. A. Viergever. 2001. Quantitative evaluation of convolution-based methods for medical image interpolation. *Med. Image Anal.* 5:111–126.

32. Kapur, J., P. K. Sahoo, and A. C. K. Wong. 1985. A new method for gray-level picture thresholding using the entropy of the histogram. *Comput. Vis. Graph. Image Process.* 29:273–285.

33. Prewitt, J. M., and M. L. Mendelsohn. 1966. The analysis of cell images. *Ann. N. Y. Acad. Sci.* 128:1035–1053.

34. Tsai, W. 1985. Moment-preserving thresholding: a new approach. *Comput. Vis. Graph. Image Process.* 29:377–393.

35. King, M. C., T. G. Drivas, and G. Blobel. 2008. A network of nuclear envelope membrane proteins linking centromeres to microtubules. *Cell.* 134:427–438.

36. Reference deleted in proof.

37. Lawrimore, J., K. S. Bloom, and E. D. Salmon. 2011. Point centromeres contain more than a single centromere-specific Cse4 (CENP-A) nucleosome. *J. Cell Biol.* 195:573–582.

38. Coffman, V. C., P. Wu, …, J. Q. Wu. 2011. CENP-A exceeds microtubule attachment sites in centromere clusters of both budding and fission yeast. *J. Cell Biol.* 195:563–572.

39. Reference deleted in proof.

40. Hachet, O., and V. Simanis. 2008. Mid1p/anillin and the septation initiation network orchestrate contractile ring assembly for cytokinesis. *Genes Dev.* 22:3205–3216.

41. Burns, D. J., and S. A. Tucker. 1977. An evaluation of fitting methods for the sum of two hyperbolas: application to uptake studies. *Eur. J. Biochem.* 81:45–52.

42. Lando, D., U. Endesfelder, …, E. D. Laue. 2012. Quantitative single-molecule microscopy reveals that CENP-A(Cnp1) deposition occurs during G2 in fission yeast. *Open Biol.* 2:120078.

43. Shivaraju, M., J. R. Unruh, …, J. L. Gerton. 2012. Cell-cycle-coupled structural oscillation of centromeric nucleosomes in yeast. *Cell.* 150:304–316.

44. Aravamudhan, P., I. Felzer-Kim, and A. P. Joglekar. 2013. The budding yeast point centromere associates with two Cse4 molecules during mitosis. *Curr. Biol.* 23:770–774.

45. Hergovich, A., D. Schmitz, and B. A. Hemmings. 2006. The human tumour suppressor LATS1 is activated by human MOB1 at the membrane. *Biochem. Biophys. Res. Commun.* 345:50–58.

46. Taniguchi, Y., P. J. Choi, …, X. S. Xie. 2010. Quantifying *E. coli* proteome and transcriptome with single-molecule sensitivity in single cells. *Science.* 329:533–538.